Vortices formation induced by femtosecond laser filamentation in a cloud chamber filled with air and helium

Yonghong Liu (刘永宏)[1,2], Haiyi Sun (孙海轶)[2,*], Jingjing Ju (鞠晶晶)[2], Ye Tian (田 野)[2], Yafeng Bai (白亚锋)[1,2], Cheng Wang (王 成)[2], Tiejun Wang (王铁军)[2], Jiansheng Liu (刘建胜)[2,3,], See Leang Chin (陈瑞良)[4], and Ruxin Li (李儒新)[2]**

[1]*MOE Key Laboratory of Advanced Micro-structured Materials, Institute of Precision Optical Engineering, School of Physics Science and Engineering, Tongji University, Shanghai 200092, China*

[2]*State Key Laboratory of High Field Laser Physics, Shanghai Institute of Optics and Fine Mechanics, Chinese Academy of Sciences, Shanghai 201800, China*

[3]*IFSA Collaborative Innovation Center, Shanghai Jiao Tong University, Shanghai 200240, China*

[4]*Center for Optics, Photonics and Laser (COPL), Laval University, Quebec City, Quebec G1V 0A6, Canada*

**Corresponding author: shy780327@siom.ac.cn; **corresponding author: michaeljs_liu@siom.ac.cn*

Received November 6, 2015; accepted January 8, 2016; posted online February 25, 2016

We report on the experimental observation of the airflow motion induced by an 800 nm, 1 kHz femtosecond filament in a cloud chamber filled with air and helium. It is found that vortex pairs with opposite rotation directions always form both below and above the filaments. We do not observe that the vortices clearly formed above the filament in air just because of the formation of smaller particles with weaker Mie scattering. Simulations of the airflow motion in helium are conducted by using the laser filament as a heat source, and the simulated pattern of vortices and airflow velocity agree well with the experimental results.

OCIS codes: 140.0140, 190.0190, 320.0320.
doi: 10.3788/COL201614.031401.

Femtosecond laser pulses could form self-guided filaments in air. It is well known that a femtosecond filamentation arises from a dynamic balance between Kerr self-focusing and self-generated plasma defocusing and/or negative higher-order Kerr terms[1–6]. In recent years, femtosecond filamentation has attracted much attention because of its potential applications, such as in pollutant detection[1,7], lightning control[8,9], laser-assisted water nucleation and snow formation[10–14], and fluid dynamic measurements[15,16], etc.

Laser-induced water condensation has been studied both in the cloud chamber and atmosphere using a 10 Hz, 220 mJ laser source[10]. Hygroscopic HNO_3 resulting from photochemically activated processes was proposed as the primary nucleation agent in the cloud chamber[10]. The formation of snow was first observed in our cloud chamber by means of high-repetition-rate (1 kHz) 800 nm, 9 mJ femtosecond laser pulses[12]. The experimental and simulated results also show that the airflow motion induced by the femtosecond laser filament, especially the formation of stable vortices, plays a significant role in water condensation and snow formation[12–14,17–19]. The humidity in the vortices is saturated or supersaturated, which would accelerate the growing of condensation nuclei and form large-sized particles into precipitation through the collisions with each other[18]. The numerical simulation results indicated that the vortices would form both above and below the filaments; however, we did not observe vortices above the filament in most of the experiments except with a very strong filament, as shown in Ref. [12]. The relevant process and mechanism need to be investigated further. In this work, we experimentally explored the airflow formation induced by 800 nm, 1 kHz femtosecond laser pulses in a cloud chamber filled with air and helium. The laser filament-induced airflow in different ambient gases was compared. The formation of vortices above the filaments is confirmed and the underlying mechanism was analyzed. The simulated results of airflow motion in helium have a good agreement with the experimental observation.

As sketched in Fig. 1, the experiments were conducted with a Ti-sapphire chirped-pulse amplification laser system (Legend Elite-Duo, Coherent, Inc.), which provided up to 8.2 mJ pulses of energy with a 30 fs pulse duration (800 nm, 1-kHz). After the beam was focused with a lens of $f = 300$ mm, it generated the filaments in the middle of the diffusion cloud chamber filled with air or helium. In order to record the 90° side Mie scattering, a continuous-wave 532 nm probe beam with 0.5 W copropagated with the femtosecond laser beam into the chamber. The probe laser was expanded by a telescope system and then truncated by a slit with dimensions of 40 mm (height) × 5 mm (width). The cloud chamber with an outside volume of 50 cm (length) × 50 cm (width) × 20 cm (height) was made of stainless steel. The vertical temperature gradient and the relative humidity (RH) inside the cloud chamber were adjusted respectively by a refrigerating machine from the underside of the cloud chamber and the electric current of a heating wire

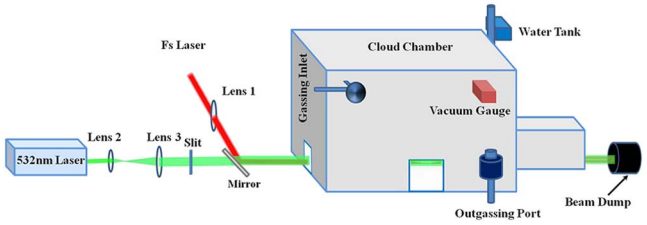

Fig. 1. Schematic of the experimental setup of the laser system and cloud chamber. The femotosecond laser beam (red line) is generated by a Ti-sapphire chirped-pulse amplification laser system and then launched into the cloud chamber via a focusing lens ($f = 300$ mm), an 800 nm highly reflective mirror, and a 3 mm-thick window (fused silica). The green laser beam (green line) expanded in diameter by Lens 2 ($f = 5$ mm) and Lens 3 ($f = 300$ mm) and truncated by a slit was used for in situ light scattering measurements by a camera (Nikon D7000).

submerged in the water reservoir. The temperature of the cooled bottom base plate of the cloud chamber was set at −46°C, while the top plate of the chamber was maintained at room temperature. The water reservoir in a 45 cm × 45 cm square frame with a cross section of 5 cm × 2 cm in a downward-pointing trough was mounted at a height of 17 cm relative to the cold bottom base plate and held distilled water pumped from a water tank above the chamber. The height of the laser axis relative to the bottom base plate of the cloud chamber was set at 10 mm, where the measured temperature and RH were about −15°C and 85%, respectively. The airflow motion around the filaments was recorded from the side window of the cloud chamber by a Nikon D7000 digital camera. When the experiment was performed in helium, the cloud chamber was evacuated to about 20 Pa and flushed three times with helium. Then, just like the experiments performed in air, the distilled water was pumped into the cloud chamber from the stainless steel reservoir, and the heating wire submerged in the water and refrigerating machine began to heat the water and cool the bottom base plate, respectively. After 20 min of cooling, femtosecond laser pulses were fired into the cloud chamber to generate the filament.

Figure 2 shows the side laser filaments captured in air and helium. As can be seen from Fig. 2, filaments with different lengths and intensities were generated in different ambient gases of air and helium. The laser filament-induced airflow motion in air and helium are illustrated respectively in Figs. 3(a) and 3(b). It can be observed that two vortices with opposite rotation formeds below the filaments both in air and helium. However, two vortices with opposite rotations also appeared above the filament in helium. The rotation direction of left and right vortices located below and above the filament is clockwise, while the direction of the other two vortex pairs is counterclockwise. The vortices below or above the filament rotate stabilize soon after the laser filament is fired. The corresponding scenarios can be seen in the supplemental movie.

We did not observe the formation of vortices above the filament in air even when the power of the probe laser was adjusted to its maximum value of 2.5 W. This probably resulted from the weaker Mie scattering induced by smaller-sized particles. In order to confirm the hypothesis, another experiment under similar experimental conditions was conducted, where the probe laser was first expanded and then focused with a cylindrical lens ($f = 650$ mm) to increase its intensity, forming a strip-shaped beam with a height of 30 mm and a width of about 2 mm. The height of the probe laser relative to the cold bottom plate of the cloud chamber could be adjusted through a translation stage. A lens with a focal length of 300 mm was used. The height of the filament was set at 10 mm to the cold plate of the cloud chamber. The vertical temperature gradient and humidity in the cloud chamber were the same as those in the experiments above. The recorded side Mie scattering of the airflow is shown in Fig. 4. The vortices above the filaments were observed when the power of probe laser was adjusted to the maximum value of 2.5 W [Fig. 4(b)]; however, under this condition, the vortices below the filaments became misty and difficult to identify due to the saturation of the scattered light. When the power of the probe laser was reduced to 0.25 W, the legible vortices below the filaments appeared again [Fig. 4(a)]. These results indicate that the vortices above the laser filaments always exist. We did not observe them in the previous experiments just because the size of scattering particles is too small, that is, there is weaker condensation above the filament. Because the refrigeration setup was installed close to the bottom plate of the cloud chamber, the temperature in the region above the filament

Fig. 2. Images of filaments in air and helium, which were captured by a digital camera (Nikon D7000: f number (F) = 5.6, light sensitivity (ISO) = 800, and shutter speed (S) = 1/13 s). The dashed line shows the position of the geometric focus. The arrows indicate the propagation direction of the femtosecond laser.

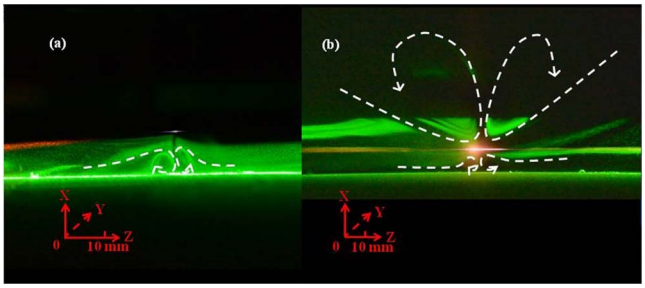

Fig. 3. Side Mie scattering images of airflow in (a) air and (b) helium, respectively, which were captured by a digital camera (Nikon D7000: F = 5.6, ISO = 800, S = 1/13 s). The white dashed curves are guidelines for the eyes for the rotation direction of the vortex pairs.

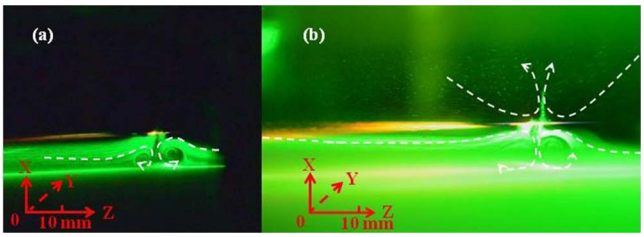

Fig. 4. Video frame figures of airflow patterns at the probe laser power of (a) 0.25 and (b) 2.5 W in the cloud chamber filled with air.

is higher and probably non-saturated, and so it is difficult for the existing cloud condensation nuclei (CCN) to grow into larger particles. In the case with the weaker probe laser, only the vortices formed below the filaments were observed because the larger particles form more easily below the filament where there is a large temperature gradient[18]. By increasing the intensity of the probe laser, the vortex motion above the filaments was observed due to the enhanced Mie scattering by the unavoidable existing particles (droplets) in the cloud chamber. In helium, the vortices above the filaments were observed because of its very light mass, and hence the larger particles that formed below the filaments could be brought upward with as the helium rose. In our early work, we observed airflow motion above the filaments only when a very strong laser filament was used[12]. A stronger laser filament accelerates the mix of airflow, and so the growth of CCN into larger particles is followed by intense Mie scattering.

In order to clarify the vortex motion in the cloud chamber, we simulated the airflow field in helium using a two-dimensional model (X–Z cross section containing a laser filament), where the laser filament is treated as a heat source[13]. The length of the filaments in helium is measured to be 12 mm, and the diameter of the filaments is 363.4 μm. The measured energy deposited by the incident laser pulse into the filaments in helium is about 1.95%, so

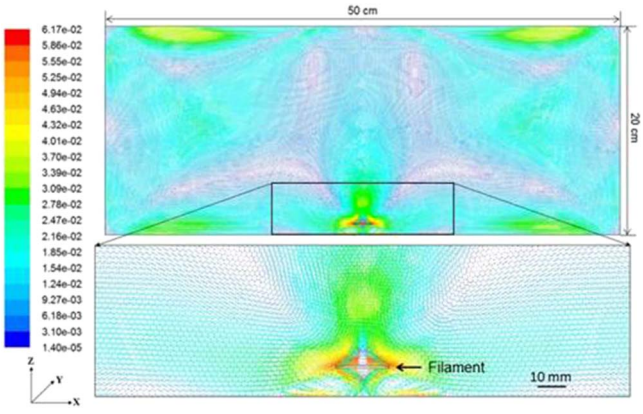

Fig. 5. Two-dimensional simulation results for airflow in the X–Z cross section (the bottom X–Y section ($Z = 0$) was the cold plate) containing laser filament in helium. The velocity vectors are colored based on their velocity magnitude (m/s).

that the calculated heat flux of the laser filament is $\sim 2.37 \times 10^4$ W/m^2 for a laser pulse energy of 8.2 mJ. The simulation results shown in Fig. 5 demonstrate that the vortices were generated both above and below the filaments in helium, and the updraft was also clearly observed above the filament. The position with the maximum airflow velocity in the simulation is located in the middle of filaments, which is also consistent with the experimental observation. The measured maximum airflow velocity around the filament is 3.34 ± 0.23 cm/s in helium by dividing the moving length of some large particles in the side scattering video by an exposure time of 1/25 s between two adjacent frames, which is close to the simulated maximum value of 6.17 cm/s. Our simulation results in air also demonstrated similar airflow patterns as those in helium, that is, vortices appeared both above and below the filaments[20]. By comparing the simulated results with experimental ones, it can be concluded that the vortices always formed above the laser filament, which was not observed in the experiments just due to the weak Mie scattering of small particles.

In conclusion, we report on the experimental observation of the airflow motion induced by femtosecond filaments in a cloud chamber filled with air and helium. The results indicate that the vortices above and below the laser filaments always form. The vortices formed above the filaments are not observed in the experiments with air just because of the formation of smaller particles followed by a weaker Mie scattering signal. We simulate the flow field in helium using a two-dimensional model, and the simulated result is consistent with the experimental observations.

This work was supported by the National Basic Research Program of China (No. 2011CB808100), the National Natural Science Foundation of China (Nos. 11425418, 61475167, 11404354, 11174305, and 61221064), the Shanghai Science and Technology Talent Project (Nos. 12XD1405200), and the State Key Laboratory Program of the Chinese Ministry of Science and Technology. Tiejun Wang also acknowledges the support from the 100 Talent Program of the Chinese Academy of Science and the Shanghai Pujiang Program.

References

1. J. Kasparian, M. Rodriguez, G. Méjean, J. Yu, E. Salmon, H. Wille, R. Bourayou, S. Frey, Y.-B. André, A. Mysyrowicz, R. Sauerbrey, J.-P. Wolf, and L. Wöste, Science **301**, 61 (2003).
2. S. L. Chin, S. A. Hosseini, W. Liu, Q. Luo, F. Théberge, N. Aközbek, A. Becker, V. P. Kandidov, O. G. Kosareva, and H. Schroeder, Can. J. Phys. **83**, 863 (2005).
3. A. Couairon and A. Mysyrowicz, Phys. Rep. **441**, 47 (2007).
4. A. Braun, G. Korn, X. Liu, D. Du, J. Squier, and G. Mourou, Opt. Lett. **20**, 73 (1995).
5. P. B. Corkum, C. Rolland, and T. Srinivasan-Rao, Phys. Rev. Lett. **57**, 2268 (1986).
6. P. Béjot, J. Kasparian, S. Henin, V. Loriot, T. Vieillard, E. Hertz, O. Faucher, B. Lavorel, and J.-P. Wolf, Phys. Rev. Lett. **104**, 103903 (2010).

7. J. Yu, D. Mondelain, G. Ange, R. Volk, S. Niedermeier, J. P. Wolf, J. Kasparian, and R. Sauerbrey, Opt. Lett. **26**, 533 (2001).
8. X. M. Zhao, J.-C. Diels, C. Y. Wang, and J. M. Elizondo, IEEE J. Quantum Electron. **31**, 599 (1995).
9. H. Schillinger and R. Sauerbrey, Appl. Phys. B **68**, 753 (1999).
10. P. Rohwetter, J. Kasparian, K. Stelmaszczyk, Z. Hao, S. Henin, N. Lascoux, W. M. Nakaema, Y. Petit, M. Queißer, R. Salamé, E. Salmon, L. Wöste, and J.-P. Wolf, Nat. Photonics **4**, 451 (2010).
11. P. Joly, M. Petrarca, A. Vogel, T. Pohl, T. Nagy, Q. Jusforgues, P. Simon, J. Kasparian, K. Weber, and J.-P. Wolf, Appl. Phys. Lett. **102**, 091112 (2013).
12. J. J. Ju, J. S. Liu, C. Wang, H. Y. Sun, W. T. Wang, X. C. Ge, C. Li, S. L. Chin, R. X. Li, and Z. Z. Xu, Opt. Lett. **37**, 1214 (2012).
13. H. Y. Sun, J. S. Liu, C. Wang, J. J. Ju, Z. X. Wang, W. T. Wang, X. C. Ge, C. Li, S. L. Chin, R. X. Li, and Z. Z. Xu, Opt. Express **21**, 9255 (2013).
14. H. Liang, H. Sun, Y. Liu, Y. Tian, J. Ju, C. Wang, and J. Liu, Chin. Opt. Lett. **13**, 033201 (2015).
15. J. B. Michael, M. R. Edwards, A. Dogariu, and R. B. Miles, Appl. Opt. **50**, 5158 (2011).
16. S. Pouya, A. Van Rhijn, M. Dantus, and M. Koochesfahani, Exp. Fluids **55**, 1791 (2014).
17. A. Ryabtsev, S. Pouya, M. Koochesfahani, and M. Dantus, Opt. Express **22**, 026098 (2014).
18. J. J. Ju, H. Y. Sun, A. Sridharan, T. J. Wang, C. Wang, J. S. Liu, R. X. Li, Z. Z. Xu, and S. L. Chin, Phys. Rev. E **88**, 062803 (2013).
19. J. J. Ju, T. Leisner, H. Y. Sun, A. Sridharan, T. J. Wang, J. W. Wang, C. Wang, J. S. Liu, R. X. Li, Z. Z. Xu, and S. L. Chin, Appl. Phys. B **117**, 1001 (2014).
20. H. Y. Sun, H. Liang, Y. H. Liu, J. J. Ju, Y. X. Wei, C. Wang, T. J. Wang, J. S. Liu, S. L. Chin, R. X. Li, and Z. Z. Xu, Appl. Phys. B **121**, 155 (2015).